Nanoscale

PAPER

How do functionalized carbon nanotubes land on, bind to and pierce through model and plasma membranes†

Lara Lacerda,‡[a] Hanene Ali-Boucetta,§[a] Sebastian Kraszewski,¶*[b] Mounir Tarek,[c] Maurizio Prato,*[d] Christophe Ramseyer,[b] Kostas Kostarelos*[a] and Alberto Bianco*[e]

Study of the mechanisms understanding how chemically functionalized carbon nanotubes internalize into mammalian cells is important in view of their design as new tools for therapeutic and diagnostic applications. The initial contact between the nanotube and the cell membrane allows elucidation of the types of interaction that are occurring and the contribution from the types of functional groups at the nanotube surface. Here we offer a combination of experimental and theoretical evidence of the initial phases of interaction between functionalized carbon nanotubes with model and cellular membranes. Both experimental and theoretical data reveal the critical parameters to determine direct translocation of the nanotubes through the membrane into the cytoplasm as a result of three distinct processes that can be summarized as landing, piercing and uptake.

1 Introduction

The study of mechanisms governing the cellular uptake of carbon nanotubes (CNTs) has been intensely addressed in the last few years.[1–5] CNTs functionalized with different therapeutic molecules can readily cross cell membranes and distribute into the different cellular compartments following alternative routes.[1,3] Two main mechanisms of uptake seem to be the prevailing ones: chemically functionalized CNTs (*f*-CNTs) able to cross the cell membrane in a direct way, translocating into

[a] Nanomedicine Lab, School of Medicine & National Graphene Institute, Faculty of Medical and Human Sciences, University of Manchester, AV Hill Building, Manchester M13 9PT, UK. E-mail: kostas.kostarelos@manchester.ac.uk

[b] Laboratoire de Nanomédecine, Imagerie et Thérapeutiques, EA 4662, Université de Franche-Comté, Centre Hospitalier Universitaire de Besançon, 25000 Besançon, France. E-mail: sebastian.kraszewski@univ-fcomte.fr

[c] UMR Structure et Réactivité des Systèmes Moléculaires Complexes, Nancy-University, CNRS, France

[d] Dipartimento di Scienze Chimiche e Farmaceutiche, Università di Trieste, Piazzale Europa 1, 34127 Trieste, Italy. E-mail: prato@units.it

[e] CNRS, Institut de Biologie Moléculaire et Cellulaire, Laboratoire d'Immunopathologie et Chimie Thérapeutique, UPR 3572, Strasbourg, 67000, France. E-mail: a.bianco@ibmc-cnrs.unistra.fr

† Electronic supplementary information (ESI) available: CNT physico-chemical characteristics, TEM images and simulation video. See DOI: 10.1039/c3nr03184e

‡ Current address: Department of Radiation Oncology, The University of Texas MD Anderson Cancer Center, 1515 Holcombe Blvd., Houston, TX 77030, USA.

§ Current address: Pharmacy, Pharmacology and Therapeutics, School of Clinical and Experimental Medicine, Medical School, University of Birmingham, Birmingham B15 2TT, UK.

¶ Current address: Laboratory of Biophysics of Macromolecular Aggregates, Institute of Biomedical Engineering and Instrumentation, Wroclaw University of Technology, PL-50377, Wroclaw, Poland, E-mail: sebastian.kraszewski@pwr.wroc.pl

the cytoplasm,[4] or an energetically active endocytotic/phagocytotic route.[3] These mechanisms are commonly coexisting during cell uptake and are strongly dependent on the type of nanotubes, the chemistry of functionalization, the charge and hydrophobic nature of the covalently linked molecules and the cell type.[1] Importantly, utilization of the ability of CNTs to translocate directly into cells has opened the way to several studies exploring the potential of these nanomaterials to develop transport vectors for therapeutics and diagnostics.[6,7]

The first step during the process of cellular uptake involves the contact between the CNTs and the lipid bilayer constituting the cellular membrane. Different theoretical studies have attempted to elucidate the behavior of CNTs coming in contact with a cellular barrier using various models of simulation.[8–13] These studies have been performed assuming pristine, non-functionalized CNTs or with nanotubes modified with small functional groups or biomolecules. Zimmerli and Koumoutsakos focused on the use of CNTs for the transportation of molecules inside the cells following the formation of transmembrane pores spanning the lipid bilayer.[8] Liu and Hopfinger showed that a nanotube interacting with a cellular membrane can lead to lipid bilayer structural reorganization and alteration as a source of possible cytotoxicity.[9] Later, Yang *et al.* demonstrated that the cytotoxic effects caused by a membrane disruption can be mitigated by doping CNTs with nitrogen atoms.[10] Recently, Kraszewski *et al.* described that nanotubes could land and float on the lipid bilayer, penetrating the lipid head-groups and sliding into the core of the membrane,[11] such behavior being dependent on the length of the tube.[12] This type of behavior is mostly driven by hydrophobic interactions as also shown for protein CNT unspecific binding.[13–17] Short functionalized CNTs were also shown to have the propensity to pierce

the lipid bilayer by a passive mechanism.[12] In contrast, Skandani et al. reported that long nanotubes were able to translocate cell membranes faster, while short tubes underwent a rotation during the final step of uptake following an endocytotic route.[18] It is evident that the characteristics of the nanotubes used in each theoretical simulation study can explain the differences found and reported, making it difficult to determine the common principles that govern CNTs cellular uptake based only on theoretical data. An attempt to correlate the theoretical studies with experimental evidence was recently reported by Shi et al.[19] Pristine nanotubes seem to enter the cells via recognition of their tips by the membrane receptors, depending on the presence or the absence of caps at the extremities of the tubes.

Another issue regarding CNTs and their interaction with model and cellular membranes is that the theoretical studies assume that it is impossible for CNTs to exit cells.[12] However, experimental studies have demonstrated that CNTs can escape from the cytoplasm by exocytosis, mediated by cell-released microvesicles.[20,21] Moreover, in mock cell experiments, conjugates formed by CNTs and small proteins, such as lysozymes, were able to induce liposome content leakage following the electrostatic interaction between the conjugate and the lipid membrane that was dependent on the liposome composition and the charge of the protein.[22] Numerous factors control the interaction between CNTs and model and cellular membranes and so far it is unclear which of these prevail at the initial step of interaction allowing successful binding and diffusion of the CNT. The hallmark of theoretical simulation studies carried out to date is the coarse-grain molecular dynamics work by Lopez et al. reporting the ability of amphiphilic organic (non-functionalized) nanotubes to penetrate a lipid bilayer in a so-called nanoneedle fashion.[23] The aim of our study here was to offer new experimental elucidation of the initial steps of interaction between biocompatible f-CNTs (relevant to biomedical applications) with model and cellular membranes.

In order to understand the role of surface charge interactions between the functional groups attached to CNTs and those on lipid bilayers, we determined the interaction between f-CNTs and liposomes (model membrane) using different experimental setups and monitoring the fluorescence spectrum and intensity of the membrane probe Nile Red. In addition, we examined f-CNTs in contact with a cell membrane at 4 °C and 37 °C by transmission electron microscopy (TEM) and finally performed an all-atom MD simulation study to describe such interactions at the atomic level.

2 Results

2.1 Positively charged CNTs interact more with negative DOPG liposomes

In order to elucidate the binding and uptake mechanism of CNTs with mammalian cells, the interactions between water dispersible f-CNTs (single- and multi-walled) and model membranes (lipid bilayers) were first studied by fluorescence spectrophotometry. For this purpose, f-CNTs were prepared following the 1,3-dipolar cycloaddition reaction, which introduces positively charged amino groups onto the external wall of
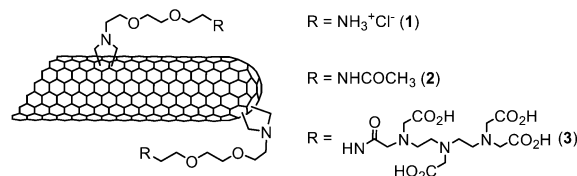

Fig. 1 Molecular structures of the different f-CNTs. (1) SWCNT–NH$_3^+$ or MWCNT–NH$_3^+$, (2) SWCNT–NH–Ac, and (3) SWCNT–DTPA.

CNTs (SWCNT–NH$_3^+$ and MWCNT–NH$_3^+$) (Fig. 1).[24,25] Part of the ammonium groups of the nanotubes were modified by acetylation (SWCNT–NH–Ac) or by introducing diaminotriethylene pentacetic anhydride (SWCNT–DTPA), thus obtaining neutral and negatively charged CNTs, respectively (Fig. 1) (see the ESI† for the physico-chemical characteristics and TEM images of the different functionalized nanotubes).

Lipid vesicles that consist of a mixture of phospholipids and cholesterol (Fig. 2) have been used as in vitro model membranes and mimic the interactions between peptides and drugs with cellular membranes.[26,27] Such vesicles are commonly known as liposomes. In addition, the incorporation of small fluorescent molecules in liposomes has been used to study the bilayer microenvironment by techniques such as spectrophotometry.[28,29]

In this study we used Nile Red (Fig. 2D), a photochemically stable, uncharged benzophenoxazone dye. Nile Red has a high partition coefficient from water to hydrophobic solvents. In addition, the presence of conjugated double bonds (delocalized electrons) allows its excitation with subsequent fluorescence emission. Due to its extremely hydrophobic characteristics, Nile Red fluoresces intensely when dissolved in organic solvents and lipids but its fluorescence is fully quenched in water.[30–33] In order to confirm the sensitivity of Nile Red to changes in solvent polarity and the resultant effect on its fluorescence characteristics, mixtures of chloroform–methanol (apolar–polar) were prepared at different volume ratios and Nile Red was added to
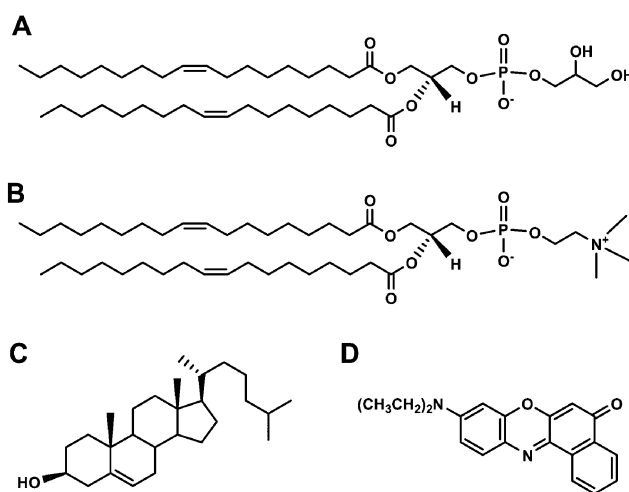
Fig. 2 Molecular structures of the lipids and organic dye used. (A) Negatively charged phospholipid DOPG, (B) zwitterionic phospholipid DOPC, (C) cholesterol, and (D) membrane dye Nile Red.

each solvent mixture (0.1 mg ml^{-1}). After scanning the fluorescence spectra of Nile Red diluted in different solvent dispersions, we observed that as the polarity of the solvent increases, the maximum fluorescence intensity of Nile Red shifts to higher wavelengths, from 600 to 637 nm and that the fluorescence intensity of Nile Red decreases by 60% of its maximum when dissolved in pure chloroform (Fig. 3).

Following this preliminary experiment, we prepared large multilamellar vesicles (liposomes) by the lipid film hydration method. Two liposome formulations were prepared by changing the phospholipid used. DOPC was used to prepare neutral model membranes while DOPG generated negatively charged model membranes. Nile Red was added to each formulation in a ratio of 1 : 300, dye : lipid molecules. We assumed that the fluorescent probe was incorporated deeply into the lipid bilayer of the liposome, thus, its spectral characteristics would reflect the polarity of the model membrane microenvironment. As expected, and in agreement with the literature[30,32] we observed that the fluorescence intensity of the dye was red-shifted (628 nm) (Fig. 4A), which indicates that the dye is not only incorporated into the membrane but is already in a more polar microenvironment than when dissolved in pure chloroform.

Subsequently, the interaction between f-CNTs and the model membranes was investigated using two differently charged multilamellar vesicles and several types of f-CNTs. Following addition of f-CNTs to aqueous suspensions of liposomes, each sample was kept for 30 min at room temperature to allow the interaction. Then, the fluorescence intensity of Nile Red was recorded (excitation wavelength of 542 nm). The effect of a gradual addition of f-CNTs to Nile Red-containing liposomes is shown in Fig. 4. We observed that the fluorescence intensity of Nile Red incorporated into neutral DOPC membranes was reduced by only 20% of the initial fluorescence intensity by the addition of SWCNT–NH$_3^+$ (Fig. 4A). In contrast, the fluorescence

intensity of Nile Red incorporated into negative DOPG membranes was reduced by up to 75% of its initial value following the addition of SWCNT–NH$_3^+$ (Fig. 4B). These results indicate that SWCNT–NH$_3^+$ were able to change the lipid bilayer microenvironment in both types of vesicles. More importantly, positively charged SWCNTs are able to interact with negatively charged lipid bilayers to a greater extent than with model membranes of neutral surface charge.

In parallel, experiments were carried out to investigate the effects of neutral (SWCNT–NH–Ac) and negatively (SWCNT–DTPA) charged nanotubes on the fluorescence intensity of Nile Red incorporated into neutral and negatively charged liposomes used as model membranes. The fluorescence intensity data were obtained, and the ratio I/I_0 (I, fluorescence reading after addition of f-CNTs; I_0, fluorescence reading in the absence of f-CNTs) was calculated and plotted versus the amount of f-CNTs added to the aqueous suspension of lipid vesicles (Fig. 4C and D). As shown in Fig. 4C, both SWCNT–NH–Ac and SWCNT–DTPA have moderate to no effect on Nile Red fluorescence intensity (modestly reduced (40%) by SWCNT–NH–Ac and minimally decreased by SWCNT–DTPA), suggesting that the nanotubes interact to a limited extent with neutral membranes. Taken together, our results demonstrate that the interaction of f-CNTs with liposomes of opposite surface charge resulted in the most prominent decrease in Nile Red fluorescence intensity, indicating that positively charged nanotubes are able to remarkably disrupt the microenvironment of negatively charged model membranes.

In order to investigate the behaviour of larger (in diameter) f-CNTs (MWCNT–NH$_3^+$) on both types of lipid vesicle model membranes, the fluorescence intensity changes of Nile Red incorporated into neutral and negatively charged lipid vesicles after the addition of MWCNT–NH$_3^+$ were analyzed. The interaction between nanotubes and vesicles of opposite surface charge resulted in the highest reduction in fluorescence intensity (about 70%, Fig. 4C and D).

These results demonstrate that electrostatic interactions play a critical role in the initial contact between f-CNTs and model membranes. Positively charged f-CNTs interacted consistently much more strongly with negatively charged DOPG lipid vesicles compared to other types of f-CNTs leading to much more significant lipid bilayer perturbations. Overall, it needs to be noted that all f-CNTs used in this study exhibited a degree of interaction with neutral DOPC vesicles.

2.2 f-CNT spatial orientation and binding to cell membranes independent of temperature

In order to understand this initial interaction between f-CNTs and the plasma membrane further, a series of experiments using TEM imaging were performed, to study the orientation and spatial conformation of the nanotubes as they approach and come in contact with cellular membranes. MWCNT–NH$_3^+$ were incubated with human lung epithelial (A549) cells for periods from 15 to 120 min at the physiologically relevant temperature of 37 °C. No cytotoxic effects such as cell detachment or blebbing were observed with the concentration of MWCNT–NH$_3^+$ used in this study. After fixing and embedding
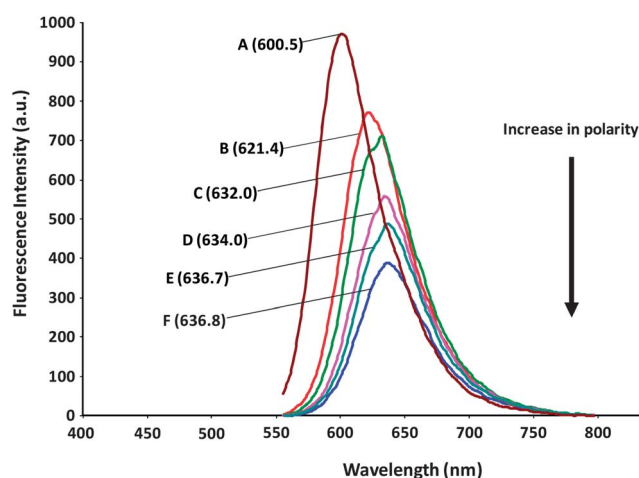
Fig. 3 Effect of solvent polarity on fluorescence spectra of Nile Red. Fluorescence spectra of Nile Red dissolved in apolar–polar (vol/vol) solvent mixtures of (A) chloroform only; (B) 8/2 chloroform–methanol; (C) 6/4 chloroform–methanol; (D) 4/6 chloroform–methanol; (E) 2/8 chloroform–methanol; (F) methanol only. The wavelength (nm) for maximum intensity is indicated for each spectrum. Excitation wavelength was 542 nm.
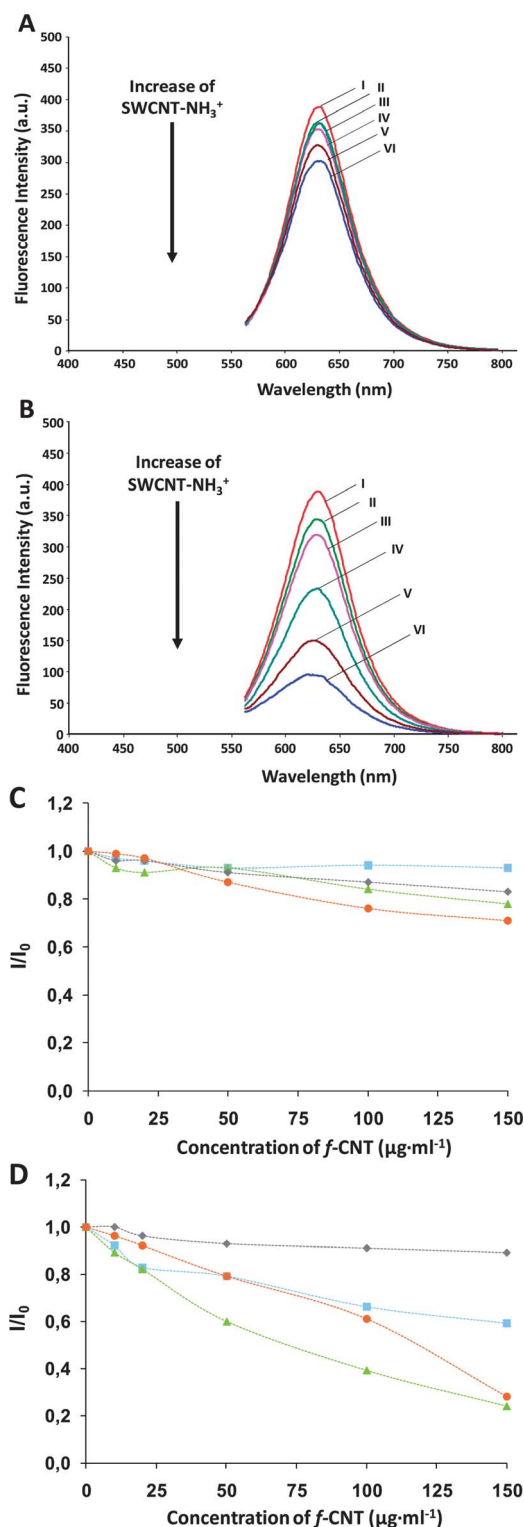
Fig. 4 Interaction of *f*-CNTs with lipid model membranes. Fluorescence spectra of Nile Red embedded in lipid bilayers exposed to increasing quantities of SWCNT–NH$_3^+$ (spectrum I to VI: 0, 10, 20, 50, 100 and 150 µg ml^{-1}): (A) DOPC liposomes; (B) DOPG liposomes. Fluorescence intensity ratio of Nile Red embedded in lipid bilayers exposed to increasing quantities (0 to 150 µg ml^{-1}) of *f*-CNTs: (C) DOPC liposomes, and (D) DOPG liposomes. Solutions were excited at 542 nm and fluorescence peak intensity values were registered at 628 nm. Grey diamond: SWCNT–DTPA; cyan square: SWCNT–NH–Ac; green triangle: SWCNT–NH$_3^+$; orange circle: MWCNT–NH$_3^+$.

the cells into EPON resin, ultra-thin sections of the cell cultures were prepared and examined by TEM. Fig. 5 shows representative images of MWCNT–NH$_3^+$ in the process of interacting with the plasma membrane.

Nanotubes reach the surface of the cell membrane in two types of orientation: either in parallel or perpendicular to the axis of the membrane (Fig. 5A–C). However, MWCNT–NH$_3^+$ seem to bind preferentially to the membrane with their longitudinal axis in parallel to the contact surface (Fig. 5D–F). These results suggest that the orientation of the CNT axis in parallel to that of the membrane offers higher surface area, with more positive functional groups able to establish stronger electrostatic interactions, and overall better binding of the nanotubes to the negatively charged cellular membrane.

In addition, the interaction of MWCNT–NH$_3^+$ with the plasma membrane was also observed at a later stage, when the nanotubes had already inserted their tip through the membrane (Fig. 5G–I). These images demonstrate that these chemically functionalized nanotubes have the ability to reorient vertically to the membrane axis, following their initial contact in a parallel orientation. In order for *f*-CNTs to be able to translocate the plasma membrane, they appear to adopt a perpendicular orientation in relation to the plasma membrane. As confirmed by the out-of-focus images (Fig. 5I), the intact nanotubes were able to pierce the cell membrane, as their tips were observed to insert through the bilayer and into the cytoplasm. Such observations are in agreement with previous work that reported *f*-CNTs capable of translocating intact through the plasma membranes and into the cytoplasm.[4,34,35]

In order to determine whether the spatial orientation between *f*-CNTs and cell membranes is energy-dependent, MWCNT–NH$_3^+$ were incubated with A459 cells also at 4 °C and studied by TEM (Fig. 6A–C).

Nanotubes were found to bind to membranes and also seen to reorient to a spatial conformation perpendicular to that of the plasma membrane, able to also insert their tip through the membrane and into the cytoplasm (Fig. 6D and E). These results further indicate that MWCNT–NH$_3^+$ interaction and orientation in relation to plasma membranes are independent of temperature.

2.3   *f*-CNT passive diffusion in three steps: landing, piercing and translocation

The experimental studies described above were complemented by simulations of functionalized SWCNTs (∼1 nm in diameter and ∼5 nm in length) with a model membrane. We have investigated using all-atom molecular dynamics (MD) simulations the interactions between amino-functionalized SWCNTs and a fully hydrated POPC membrane. This theoretical method is one of the most efficient ways to reveal the molecular mechanisms at initiating CNT cellular uptake. The model nanotube contains seven amino groups (one every 86 carbon atoms) randomly distributed onto the CNT surface, thus directly agreeing with the experimental *f*-CNT (**1**) shown in Fig. 1 (similar degree of functionalization). Representative snapshots of MD runs illustrated *f*-CNT translocation by passive diffusion as can be seen in Fig. 7.
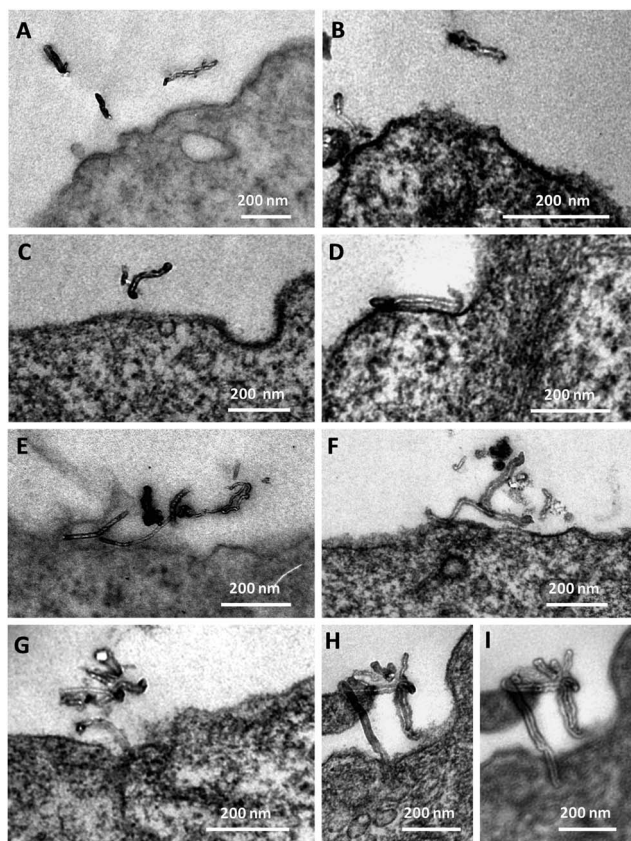
Fig. 5 Interaction of MWCNT–NH$_3^+$ with plasma membranes at 37 °C. TEM images of MWCNT–NH$_3^+$ incubated with A549 cells at 37 °C. (A–C) MWCNT–NH$_3^+$ approaching the membrane, (D–F) MWCNT–NH$_3^+$ binding to the membrane, and (G–I) MWCNT–NH$_3^+$ crossing the membrane. Image I is an out-off focus image of H, to show the MWCNT–NH$_3^+$ structure beyond the plasma membrane.
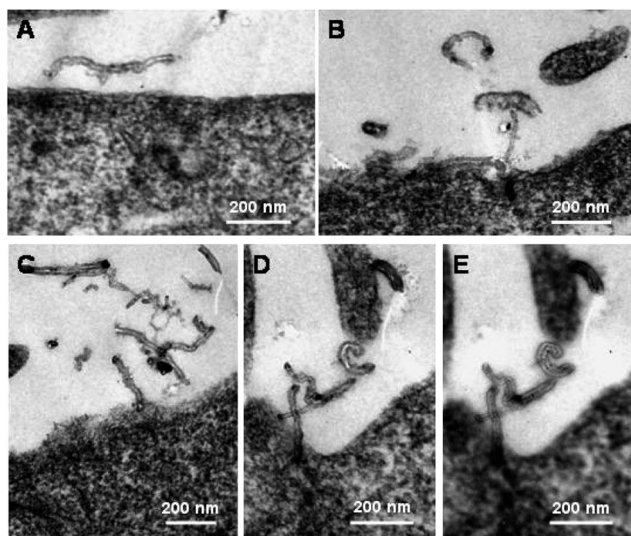

Fig. 6 Interaction of MWCNT–NH$_3^+$ with plasma membranes at 4 °C. TEM images of MWCNT–NH$_3^+$ incubated with A549 cells at 4 °C. (A–C) MWCNT–NH$_3^+$ approaching and binding the membrane, and (D & E) MWCNT–NH$_3^+$ crossing the membrane. Image E is an out-off focus image of D, to show the MWCNT–NH$_3^+$ structure beyond the plasma membrane.

Such diffusion can be distinguished into three distinct processes: (1) surface landing, (2) membrane piercing, and (3) translocation. First, a *f*-SWCNT approached the membrane at an angle α of about 20° with respect to the normal direction of the bilayer plane (Fig. 8A). After 30 ns, landing occurred and *f*-CNT remained parallel to the membrane interface for over 180 ($\alpha = 90°$). At ∼200 ns, the *f*-SWCNT reoriented with respect to the membrane at an angle ∼15° then, as a nanoneedle, dove into its hydrophobic core, dragging with it water molecules (Fig. 8B). Finally, the *f*-SWCNT was uptaken into the membrane core (at ∼340 ns) and stayed in this configuration until the end of simulation (424 ns). The number of water molecules present in the hydrophobic core of membrane increased locally by about 40% during *f*-SWCNT insertion. This could be the origin of membrane disruption. A detailed illustration of the *f*-SWCNT insertion process into the lipid bilayer can also be seen in the video provided in the ESI.†

From the simulation performed, the complete translocation of intact *f*-SWCNTs through the lipid bilayer could not be observed. This was probably due to the charge interactions between the functional parts of the CNT and the lipid heads. It can be assumed that for *f*-SWCNT to translocate intact through the whole plasma membrane a deprotonation/reprotonation mechanism must occur similar to that previously described for charged amino-functionalized fullerenes.[36] Our MD simulation did not incorporate such deprotonation/reprotonation mechanisms.

3   Discussion

Although several studies have reported the internalization of CNTs by eukaryotic and mammalian cells, the initial interactions, the factors determining such interactions and how the CNTs enter cells are still unclear and mainly addressed by theoretical calculations.[8–19] In this study we have attempted to correlate the experimentally determined binding of *f*-CNTs with model membranes (lipid vesicles) and plasma membranes (A549 cells) with the interactions obtained by molecular dynamics simulations. We conclude that electrostatic interactions between the hydrophilic and charged functional moieties of *f*-CNTs and the polar headgroups of the lipid vesicles are the major contributors to the overall initial interaction. Furthermore, our experimental observations were found to be in good agreement with theoretical work by Lopez *et al.* showing that an amphiphilic nanotube (3 nm length and 1.3 nm diameter) with
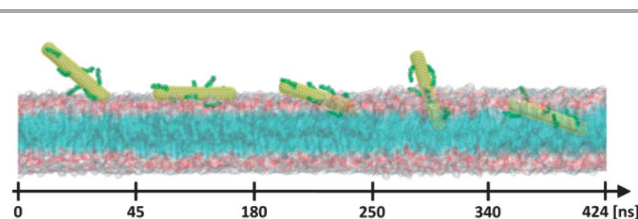
Fig. 7 Consecutive snapshots issued from unconstrained MD simulation of *f*-CNT diffusing passively to the lipid membrane. The molecular mechanism of interaction can be divided into three main processes: (1) landing (up to 180 ns), (2) nanoneedle like picking (up to 340 ns), and (3) uptake.
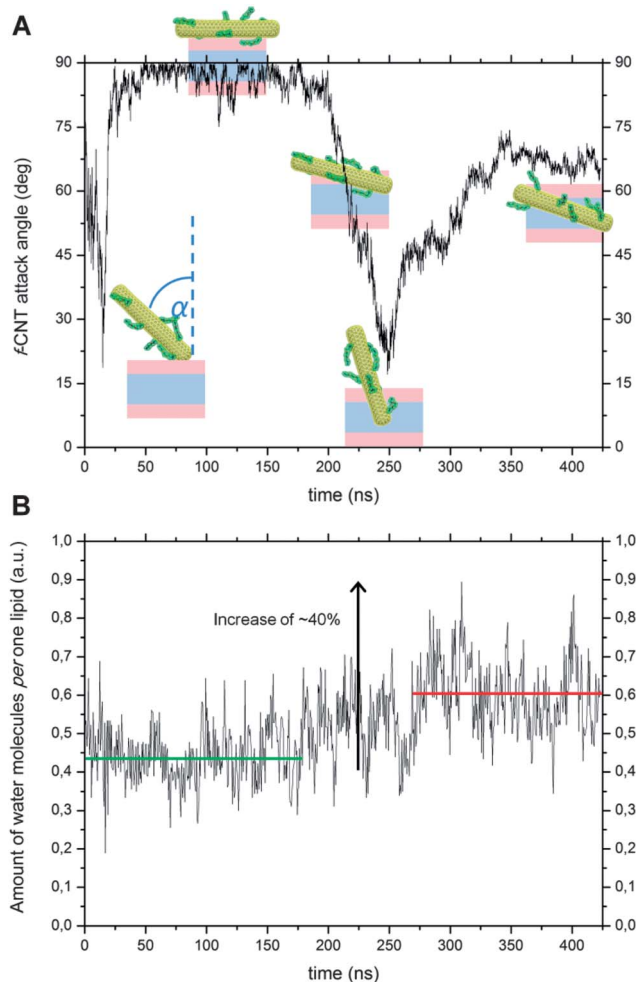
Fig. 8 Behavior of water and f-CNT during lipid insertion. (A) f-SWCNT attack angle (α) with respect to the normal of the membrane plane, as a function of simulation time during its translocation. (B) Number of water molecules present in the hydrophobic core of the membrane increases from 0.43 (per one lipid molecule) to about 0.60 during f-SWCNT insertion.

hydrophilic functional groups localized at its terminus spontaneously insert into a lipid bilayer in a two-step mechanism: (a) the nanotube is adsorbed onto the membrane surface, and (b) it reorients spontaneously and adopts a transmembrane configuration.[23] Our data are also in agreement with those recently reported by Shi *et al.*[19] These authors attempted to correlate the risks of CNT length-dependent toxicity to the mechanisms of cell uptake to design safer nanotubes.[37] The interactions of non-functionalized multi-walled carbon nanotubes with cell membranes were elucidated experimentally and theoretically. Similar to our results, the nanotubes enter the cells through the tip. In particular, the tips of nanotubes with closed extremities are initially recognized by and bind to cell membrane receptors, subsequently leading to a rotation of the tube and an almost vertical entry.[19]

The reduction in the fluorescence intensity of Nile Red incorporated into our DOPG model membrane indicate that the bilayer environment was more polar after the gradual addition of positively charged CNTs to the negatively charged

membrane. Thus, the increase of polarity within the bilayer microenvironment is likely due to the interaction, binding and eventual piercing of the f-CNTs through the model membrane. For these reasons, we concluded that CNT–NH$_3^+$ interact primarily through attractive electrostatic forces to approach and adsorb onto model membranes. However, if the hydrophobic dye is deeply incorporated in the bilayer, further events must develop after the binding step to promote the quenching of the dye. We speculate that the f-CNTs penetrated the lipid membrane and caused a concomitant introduction of water molecules in the lipid bilayer hydrophobic space that increased its polarity.

Earlier we showed that the cellular uptake of functionalized carbon nanotubes is independent of functional group and cell type.[4] In the present work, studies on model membranes were complemented by TEM studies of the initial interactions of nanotubes with plasma membranes using mammalian cells. We observed that MWCNT–NH$_3^+$ initially interacted with cell membranes with their long axis in parallel to the plasma membrane axis, but later they reoriented perpendicular to the plasma membrane and inserted their tips through. Furthermore, our results showed that the process of f-CNTs diffusion through cell membranes was not dependent on the temperature at which the cells were incubated with f-CNTs. Such results are in agreement with previously published experimental[1,4,38] and theoretical[11] work that showed f-CNTs are able to pierce cell membranes by passive diffusion.

Lastly, the MD simulations performed indicate that CNT diffusion through membranes can occur in three distinct processes: (1) landing, (2) piercing, and (3) uptake, that summarized all the experimental work described. In conclusion, the present studies provided experimental evidence confirmed by MD simulations, suggesting that chemically functionalized, biocompatible CNTs must have hydrophilic and positively charged moieties in order to maximize interactions and bind with the moderately negatively charged plasma membranes. Following binding, the nanotubes are able to reorient perpendicular to the axis of the membrane and finally allow hydrophobic interactions to pierce the lipid bilayers of the membranes that can lead to translocation of the nanotube. Overall, a fine balance between surface charge characteristics of the nanotube appended functional groups and the exposure of the hydrophobic domains of the carbon backbone seem to be responsible for the molecular interactions with plasma membrane components that can lead to their direct translocation through the membrane and into the cytoplasm.

4 Experimental section

4.1 CNTs

Pristine HiPco SWCNTs were purchased from Carbon Nanotechnologies Inc. (Lot No.: R0496). According to the manufacturer, the mean diameter of SWCNTs is about 1 nm. Tubes have lengths between 300 and 1000 nm. Pristine MWCNTs were obtained from Nanostructured and Amorphous Materials Inc. (Lot No.: 1240XH, 94% pure, outer diameters between 20 and 30 nm, and lengths between 0.5 and 2 μm).

4.2 Functionalization of CNTs

Single- and multi-walled ammonium-functionalized CNTs (SWCNT–NH_3^+ and MWCNT–NH_3^+) were synthesized by a 1,3-dipolar cycloaddition reaction as previously reported.[24,25] Acetamido-functionalized CNT (SWCNT–NH–Ac) were prepared as described in ref. 39. DTPA-functionalized CNT (SWCNT–DTPA) were prepared as reported in ref. 40.

Following the functionalization by the 1,3-dipolar cycloaddition reaction, CNTs with ammonium moieties were readily soluble in deionized water at relatively high concentrations (5–10 mg ml^{-1}). Additional modification with acetyl groups slightly reduced the solubility of CNTs, while the modification with DTPA did not change the solubility of CNTs compared the precursor nanotubes with ammonium groups. Stock dispersions were prepared by hydration of each type of f-CNT in deionized water at concentrations of 6.7 mg ml^{-1} (MWCNT–NH_3^+), 6 mg ml^{-1} (SWCNT–NH_3^+) and 3 mg ml^{-1} (SWCNT–Ac and SWCNT–DTPA) under mild sonication using a water bath. All dispersions were kept at 4 °C until needed and always sonicated before used.

4.3 Model membrane (liposome) preparation

Liposomes were prepared by the lipid film hydration method. Briefly, phospholipids DOPG [1,2-dioleoyl-sn-glycero-3-[phospho-rac-(1-glycerol), from Sigma] and DOPC (1,2-dioleoyl-sn-glycero-3-phosphocholine, from Avanti) and cholesterol (Sigma) were dissolved in chloroform–methanol (4 : 1 vol/vol) at a final total lipid concentration of 2 mM of which 10 mol% was cholesterol. Nile Red (membrane probe) was added to the lipid mixture in a ratio of 1 : 300 lipid molecules. After evaporation of the organic solvents, the lipid film was hydrated with 1 ml saline solution (0.09% NaCl) and vortexed for 15 min to achieve a final concentration of 2 mM. Following hydration, large multi-lamillar liposomes were obtained. All liposome suspensions were kept at 4 °C until needed.

4.4 Fluorescence intensity studies

f-CNTs were added to 50 μg of liposomes (DOPG and DOPC) and rapidly mixed. The suspension mixtures were incubated at room temperature for 30 min and then fluorescence emission of Nile Red was scanned on a Perkin Elmer LS 50B spectrophotometer. Quartz cuvettes with a path length of 4 cm were used. Samples were excited at 542 nm and emission scans were recorded from 550 to 800 nm.

4.5 Transmission electron microscopy studies

In order to investigate the cellular interaction of f-MWCNTs by transmission electron microscopy (TEM), A549 cells were seeded in Millicell® plate inserts (12 mm, polycarbonate membrane, 0.4 μm pore size), 3 days prior the experiment. Then, after being washed with PBS, the cells were incubated with MWCNT–NH_3^+ (50 μg ml^{-1}) at 37 °C or 4 °C for 15, 30, 60 and 120 min in serum-free media. Cells were then rewashed with PBS and fixed with 3% glutaraldehyde in 0.1 M cacodylate buffer (pH 7.4) at 4 °C overnight. On the following day, after

washing the cells 3 times with distilled water, a secondary fixation was carried out with 1% aqueous osmium tetroxide (OsO_4) for 60 min. The cells were then rinsed with water and dehydrated in a series of ethanol solutions (70%, 90% and 100%). Infiltration with araldite resin (Agar, UK) was carried out using a 1 : 1 mixture of ethanol and araldite resin mix (2 times for 15 minutes each) and neat resin (2 h). The wells were filled with fresh resin and placed into the oven to polymerise the resin at 60 °C for 48 h. Ultra-thin sections (65–85 nm thick) were stained with uranyl acetate and lead citrate, and imaged with a Philips CM10 TEM at 80 kV. Images were captured with a high resolution digital camera.

4.6 Molecular dynamics simulations

Unconstrained full atomistic molecular dynamics (MD) simulations were performed using an equilibrated, fully hydrated zwitterionic POPC (palmitoyl-oleoyl-phosphatidylcholine) membrane model. At the temperature set for the study, i.e. 300 K, the bilayer is in the biologically relevant liquid-crystalline (Lα) phase. The simulation box consists of 180 POPC units, 14 512 water molecules and one water-soluble closed (6,6) SWCNT (∼1 nm in diameter and ∼5 nm in length). Such a small length of f-CNT was chosen to perform a quantitative simulation within a sufficient timeframe (424 ns). The functionalized CNT contains 7 ammonium groups (f-SWCNT–NH_3^+) randomly distributed on the whole surface (one functional group per 86 carbon atoms). The initial dimensions of the simulation box of $7.0 \times 7.4 \times 12.6$ nm^3 were chosen to ensure a reasonable thickness of the water layers on both sides of the membrane (8.6 nm taking into account periodic boundary conditions). This is also large enough to accommodate the 5.3 nm long f-CNT which was used in the MD study. The system neutrality was guaranteed by adding 7 chlorine counter ions. All MD simulations were carried out using NAMD2.6,[41] a program targeted for massively parallel architectures. Short- and long-range forces were calculated every 1 and 2 time-steps respectively, with an integration time of 2.0 fs. The Langevin dynamics algorithm and the Langevin piston Nosé–Hoover method[42] were used to maintain constant 300 K temperature and 1 bar pressure in the system. Long-range electrostatic forces were taken into account using the particle mesh Ewald (PME) approach.[43] The force field parameters for the lipid are taken from CHARMM27 (ref. 44) with the united atoms extension. The intra- and intermolecular potentials for water are modeled within the TIP3P approach.[45] For the CNT carbon–carbon or carbon–water interactions, we followed Bedrov's description[46] (CHARMM27 functionals: σCC = 3.895 Å, εCC = 0.066 kcal mol^{-1} and σCO = 3.580 Å, εCO = 0.0936 kcal mol^{-1}). Necessary interaction parameters of the ammonium group (electrostatics and force constants) were extracted from ab initio calculations. We used the Gaussian03 package software[47] to evaluate the effective electrostatic potential. The RHF//6-31+G level of theory was considered together with the polarized continuum water model (integral equation formalism IEFPCM) in order to reproduce the environmental effect of the solvent. Supplementary analysis based on construction of the Hessian matrix (the matrix of second

derivatives of the energy with respect to geometry) was also performed to extract the force constants between atoms in the ammonium group. The derived partial charges (Mulliken charge distributions)[48] were then applied in the MD simulations, according to the results obtained from the quantum mechanics calculations. Following quantum mechanical calculations, a large scale MD simulation was performed. First, the stability of the *f*-CNT was tested in the water box in order to find a stable equilibrated structure before inserting it to the system containing the hydrated POPC lipid bilayer. Next, the *f*-CNT was placed in the bulk water parallel and not closer than 5 Å to the membrane surface.

Acknowledgements

References

1 L. Lacerda, J. Russier, G. Pastorin, M. A. Herrero, E. Venturelli, H. Dumortier, K. T. Al-Jamal, M. Prato, K. Kostarelos and A. Bianco, *Biomaterials*, 2012, **33**, 3334.

2 V. Raffa, G. Ciofani, O. Vittorio, C. Riggio and A. Cuschieri, *Nanomedicine*, 2010, **5**, 89.

3 N. W. Kam, Z. Liu and H. Dai, *Angew. Chem., Int. Ed.*, 2006, **45**, 577.

4 K. Kostarelos, L. Lacerda, G. Pastorin, W. Wu, S. Wieckowski, J. Luangsivilay, S. Godefroy, D. Pantarotto, J.-P. Briand, S. Muller, M. Prato and A. Bianco, *Nat. Nanotechnol.*, 2007, **2**, 108.

5 M. H. Lamm and P. C. Ke, *Methods Mol. Biol.*, 2010, **625**, 135.

6 K. Kostarelos, A. Bianco and M. Prato, *Nat. Nanotechnol.*, 2009, **4**, 627.

7 Z. Liu, S. Tabakman, K. Welsher and H. Dai, *Nano Res.*, 2009, **2**, 85.

8 U. Zimmerli and P. Koumoutsakos, *Biophys. J.*, 2008, **94**, 2546.

9 J. Liu and A. J. Hopfinger, *Chem. Res. Toxicol.*, 2008, **21**, 459.

10 Y. Yang, X. Li, J. Jiang, H. Du, L. Zhao and Y. Zhao, *ACS Nano*, 2010, **4**, 5755.

11 S. Kraszewski, A. Bianco, M. Tarek and C. Ramseyer, *PLoS One*, 2012, e40703.

12 S. Kraszewski, F. Picaud, I. Elhechmi, T. Gharbi and C. Ramseyer, *Carbon*, 2012, **50**, 5301.

13 J.-W. Shen, T. Wu, Q. Wang and Y. Kang, *Biomaterials*, 2008, **29**, 3847.

14 G. Zuo, Q. Huang, G. Wei, R. Zhou and H. Fang, *ACS Nano*, 2010, **4**, 7508.

15 G. Zuo, W. Gu, H. Fang and R. Zhou, *J. Phys. Chem. C*, 2011, **115**, 12322.

16 M. Calvaresi, S. Hoefinger and F. Zerbetto, *Chem.–Eur. J.*, 2012, **18**, 4308.

17 F. De Leo, J. Sgrignani, D. Bonifazi and A. Magistrato, *Chem.–Eur. J.*, DOI: 10.1002/chem.201301376.

18 A. A. Skandani, R. Zeineldin and A. Al-Haik, *Langmuir*, 2012, **28**, 7872.

19 X. Shi, A. von den Bussche, R. H. Hurt, A. B. Kane and H. Gao, *Nat. Nanotechnol.*, 2011, **6**, 714.

20 H. Jin, D. A. Heller and M. S. Strano, *Nano Lett.*, 2008, **8**, 1577.

21 I. Marangon, N. Boggetto, C. Ménard-Moyon, E. Venturelli, M.-L. Beoutis, C. Péchoux, N. Luciani, C. Wilhelm, A. Bianco and F. Gazeau, *Nano Lett.*, 2012, **12**, 4830.

22 A. Hirano, K. Uda, Y. Maeda, T. Akasaka and K. Shiraki, *Langmuir*, 2010, **26**, 17256.

23 C. F. Lopez, S. O. Nielsen, P. B. Moore and M. L. Klein, *Proc. Natl. Acad. Sci. U. S. A.*, 2004, **101**, 4431.

24 V. Georgakilas, K. Kordatos, M. Prato, D. M. Guldi, M. Holzinger and A. Hirsch, *J. Am. Chem. Soc.*, 2002, **124**, 760.

25 V. Georgakilas, N. Tagmatarchis, D. Pantarotto, A. Bianco, J.-P. Briand and M. Prato, *Chem. Commun.*, 2002, 3050.

26 F. Reig, I. Haro, D. Polo, M. A. Egea and M. A. Alsina, *J. Colloid Interface Sci.*, 2002, **246**, 60.

27 M. Kepczynski, A. Karewicz, A. Gornicki and M. Nowakowska, *J. Phys. Chem. B*, 2005, **109**, 1289.

28 E. Perochon, A. Lopez and J. F. Tocanne, *Biochemistry*, 1992, **31**, 7672.

29 A. S. Klymchenko, G. Duportail, A. P. Demchenko and Y. Mely, *Biophys. J.*, 2004, **86**, 2929.

30 P. Greenspan and S. D. Fowler, *J. Lipid Res.*, 1985, **26**, 781.

31 A. K. Dutta, K. Kamada and K. Ohta, *J. Photochem. Photobiol., A*, 1996, **93**, 57.

32 K. Kostarelos, P. F. Luckham and T. F. Tadros, *J. Colloid Interface Sci.*, 1997, **191**, 341.

33 M. M. G. Krishna, *J. Phys. Chem. A*, 1999, **103**, 3589.

34 D. Pantarotto, R. Singh, D. McCarthy, M. Erhardt, J.-P. Briand, M. Prato, K. Kostarelos and A. Bianco, *Angew. Chem., Int. Ed.*, 2004, **43**, 5242–5246.

35 J. Rojas-Chapana, J. Troszczynska, I. Firkowska, C. Morszeck and M. Giersig, *Lab Chip*, 2005, **5**, 536.

36 S. Kraszewski, M. Tarek and C. Ramseyer, *ACS Nano*, 2011, **5**, 8571.

37 H. Ali-Boucetta, A. Nunes, R. Sainz, M. A. Herrero, B. Tian, M. Prato, A. Bianco and K. Kostarelos, *Angew. Chem., Int. Ed.*, 2013, **52**, 2274.

38 D. Pantarotto, J.-P. Briand, M. Prato and A. Bianco, *Chem. Commun.*, 2004, 16.

39 L. Lacerda, G. Pastorin, W. Wu, M. Prato, A. Bianco and K. Kostarelos, *Adv. Funct. Mater.*, 2006, **16**, 1839.

40 R. Singh, D. Pantarotto, L. Lacerda, G. Pastorin, C. Klumpp, M. Prato, A. Bianco and K. Kostarelos, *Proc. Natl. Acad. Sci. U. S. A.*, 2006, **103**, 3357.

41 J. C. Phillips, R. Braun, W. Wang, J. Gumbart, E. Tajkhorshid, E. Villa, C. Chipot, R. D. Skeel, L. Kalé and K. Schulten, *J. Comput. Chem.*, 2005, **26**, 1781.

42 S. E. Feller, Y. Zhang, R. W. Pastor and B. R. Brooks, *J. Chem. Phys.*, 1995, **103**, 4613.

43 T. Darden, D. York and L. Pedersen, *J. Chem. Phys.*, 1993, **98**, 10089.

44 N. Foloppe and A. D. MacKerell, *J. Comput. Chem.*, 2000, **21**, 86.

45 W. L. Jorgensen, J. Chandrasekhar, J. D. Madura, R. W. Impey and M. L. Klein, *J. Chem. Phys.*, 1983, **79**, 926.

46 L. W. Li, H. Davande, D. Bedrov and G. D. Smith, *J. Phys. Chem. B*, 2007, **111**, 4067.

47 M. J. Frisch, G. W. Trucks, H. B. Schlegel, G. E. Scuseria, M. A. Robb, *et al.*, *Gaussian 03 (Revision C.02)*, Gaussian, Inc., Wallingford CT, 2004.

48 R. S. Mulliken, *J. Chem. Phys.*, 1955, **23**, 1833.